Accepted Manuscript

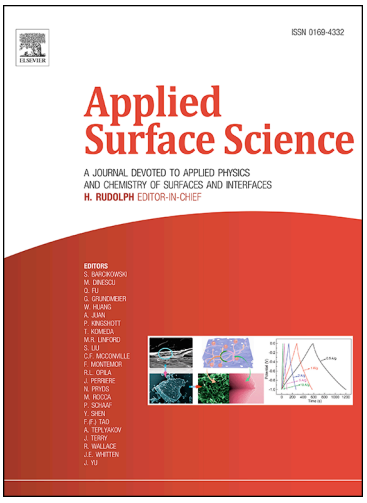

Full Length Article

Chemical synthesis of flexible nanoflakes-like $NiCo_2S_4$ electrodes for high-performance supercapacitor application

S.K. Shinde, M.B. Jalak, G.S. Ghodake, N.C. Maile, V.S. Kumbhar, D.S. Lee, V.J. Fulari, D.-Y. Kim

PII: S0169-4332(18)32856-3
DOI: https://doi.org/10.1016/j.apsusc.2018.10.100
Reference: APSUSC 40668

To appear in: *Applied Surface Science*

Received Date: 9 June 2018
Revised Date: 6 September 2018
Accepted Date: 11 October 2018

Please cite this article as: S.K. Shinde, M.B. Jalak, G.S. Ghodake, N.C. Maile, V.S. Kumbhar, D.S. Lee, V.J. Fulari, D.-Y. Kim, Chemical synthesis of flexible nanoflakes-like $NiCo_2S_4$ electrodes for high-performance supercapacitor application, *Applied Surface Science* (2018), doi: https://doi.org/10.1016/j.apsusc.2018.10.100

Chemical synthesis of flexible nanoflakes-like $NiCo_2S_4$ electrodes for high-performance supercapacitor application

S. K. Shinde[a], M. B. Jalak[ab], G. S. Ghodake[a], N. C. Maile[b], V. S. Kumbhar[c], D. S. Lee[d], V. J. Fulari[b], D.-Y. Kim[a]*

[a]*Department of Biological and Environmental Science, College of Life Science and Biotechnology, Dongguk University, 32 Dongguk-ro, Biomedical Campus, Ilsandong-gu, Siksa-dong, 10326, Goyang-si, Gyeonggi-do, South Korea*

[b]*Holography and Materials Research Laboratory, Department of Physics, Shivaji University, Kolhapur-416004, Maharashtra, India*

[c]*School of Nano & Materials Science and Engineering, Department of Energy Chemical Engineering, Kyungpook National University, 2559 Gyeongsang-daero Sangju, Gyeongbuk, South Korea*

[d]*Department of Environmental Engineering, Kyungpook National University, 80 Daehak-ro, Buk-gu, Daegu 41566, South Korea*

*Corresponding author.

Tel: +82-31-961-5122

Fax: +82-31-961-5122

Mobile: +82-10-6658-5213

E-mail: sbpkim@dongguk.edu (Prof. D.-Y. Kim)

Abstract

In this paper, we synthesized several nanostructures, including nanoflakes-, nanosheets-, and nanopetals-like $NiCo_2S_4$ flexible electrodes on a flexible stainless-steel substrate, by using successive ionic layer adsorption and reaction method for high-performance supercapacitor application. The as-prepared $NiCo_2S_4$ electrodes were structurally and morphologically characterized by X-ray diffraction (XRD), field emission scanning electron (FE-SEM) microscopy, transmission electron (TEM) microscopy, and the supercapacitance evaluated using electrochemical measurements. The nanoporous, three-dimensional interconnected nanosheets-like $NiCo_2S_4$ arrays are excellent candidate electrodes for supercapacitor application, demonstrating a high specific capacitance, and long time charge/discharge ability. The calculated values of specific capacitance shows the number of deposition cycles influences the surface morphology, which is confirmed by the FE-SEM and electrochemical testing, displaying a capacitance of 766, 1076, and 921 F g^{-1}, for 5, 9, and 14 cycles, respectively. The supercapacitor performance confirmed the size of the nanoflakes is appropriate to prepare $NiCo_2S_4$ electrodes for high-rate electrochemical supercapacitive energy storage devices.

Keywords: SILAR method, nanostructure size, supercapacitor, capacitance, cyclic stability.

1. Introduction

Worldwide, research is increasingly focusing on portable, safe, renewable energy storage electrical devices and lightweight electronic devices, like supercapacitors, which provide environmental stability, as well as high power and energy densities [1-9]. The supercapacitor is superior to the capacitor and batteries because of its capability to store power and energy densities [1, 10-14]. Supercapacitors are essentially divided into three main categories: electric double-layer capacitors, electrochemical pseudocapacitors, and hybrid capacitors [3, 15, 16]. In recent years, various binary and ternary transition metal oxides have been used for supercapacitors, due to the rich redox reaction at the surface/electrolyte interfaces [6-9, 17-19].

Several researchers are working on the binary and ternary metal oxides/sulfides, like NiS, CoS, $NiCoO_4$, and $NiCoS_4$ compounds, as electrode materials in supercapacitors. These materials are prepared using methods, such as hydrothermal [9, 20], co-electrospinning [21], solvothermal [22], chemical liquid [23], electrodeposition [24], microwave-assisted [25], hydrothermal/solvothermal [26], co-precipitation [27], one-pot refluxing [28], solvothermal method [29], soft-template [30], and freeze-drying [31]. Several of these deposition techniques are used to synthesize $NiCoS_4$ nanomaterials for the electrochemical supercapacitor application. In this paper, we used the SILAR method to synthesize nanomaterials for supercapacitor application. Besides being low-cost, simple, and eco-friendly, the SILAR technique is more economically stable and allows for a greater number of applications than other physical and chemical methods.

$NiCo_2S_4$-based electrodes are excellent candidates for electrochemical testing, due to their physical and electrochemical applications [32]. He et al. [33] produced $NiCo_2S_4$@Ni_3S_2 core–shell nanotube arrays as electrodes in asymmetric $NiCo_2S_4$@Ni_3S_2//reduced graphene oxide

supercapacitors, using a facile and commendable method on Ni foam. Niu and coworkers [34] combined a hydrothermal process with a co-precipitation approach to synthesize $NiCo_2S_4$@$Ni_3V_2O_8$ nanomaterials on nickel foam and observed that $NiCo_2S_4$@$Ni_3V_2O_8$ possesses a better specific capacitance of 512 C g^{-1} at 1 A g^{-1} current density. The authors concluded that $NiCo_2S_4$ electrodes are potential candidates for supercapacitor energy storage applications. Wu et al. [35] successfully fabricated $NiCo_2S_4$@C thin films by a facile in situ template removal method and concluded that the $NiCo_2S$@C is a promising candidate for supercapacitor properties, exhibiting a specific capacitance of 1592 mA g^{-1}. Yao et al. [36] prepared $NiCo_2S_4$@$NiMoO_4$ core–shell nanospheres, with the same intention. The $NiCo_2S_4$@$NiMoO_4$ core–shell nanospheres displayed a specific capacitance of 1740 mF cm^2 at 1 mA cm^{-2}. Nonetheless, to the greatest of our knowledge, there are no prior reports on $NiCo_2S_4$ thin films for the electrochemical testing of supercapacitor applications, using the SILAR method.

In this paper, we report the influence of the SILAR cycle on the supercapacitor performance of nanoflakes-, nanosheets-, and nanoplates-like $NiCo_2S_4$ electrodes, based on their physical and electrochemical properties. Subsequently, the electrochemical performance of the $NiCo_2S_4$ electrodes was studied to determine the specific capacitance. Especially, the nanosheets-like $NiCo_2S_4$ nanostructure displays a higher specific capacitance of 1076 F g^{-1}. Additionally, the $NiCo_2S_4$ electrode provides low resistance, indicating the excellent current conduction of the electrode. In the discussion, interconnected nanosheets-like $NiCo_2S_4$ electrodes are demonstrated to be suitable for supercapacitor applications.

2. Experimental Details

2.1 Materials

1.05 g $NiSO_4.6H_2O$, 2.25 g $CoSO_4.7H_2O$, 1.35 g $Na_2S.5H_2O$, and liquid ammonium hydroxide (NH_4OH).

2.2 Synthesis of $NiCo_2S_4$ nanosheets

In a typical process, 1.05 g $NiSO_4.6H_2O$, 2.25 g $CoSO_4.7H_2O$, and 1.35 g $Na_2S.5H_2O$ were dissolved separately in 40 mL of double-distilled water (DDW). After magnetic stirring for 20 min, all solutions were uniform and transparent. The growth of nanosheets-like $NiCo_2S_4$ on flexible stainless-steel substrate was realized in a three-step process, by using the SILAR method. A stainless-steel substrate (2×5 cm) was polished using various polish papers before deposition. To remove the oily surface, the substrate was initially cleaned with 1 M H_2SO_4, followed by ultrasonic treatment. In the first step, the flexible stainless-steel substrate was immersed in $NiSO_4$ solution for 20 s, to allow adsorption of Ni^{2+} ions on the surface of the substrate. The Ni^{2+}-coated substrate was rinsed with DDW for 10 s, to remove loosely bound Ni^{2+} species. In the second step, the Ni^{2+}-coated substrate was immersed in $CoSO_4$ solution for 20 s, enabling the adsorption of Co^{2+} ions onto the surface of the Ni^{2+}-coated substrate. A similar process to that described above for removal of Ni^{2+} species was applied to remove loosely bound Co^{2+} ions. Then, in the third and final step, the Ni^{2+}/Co^{2+}-coated flexible stainless-steel substrate was immersed in Na_2S precursor solution. The $Ni^{2+}+Co^{2+}+S^{2-}$-coated substrate was rinsed with DDW for 10 s, to remove roughly bound S^{2-} ion species. Consequently, one SILAR cycle of $NiCo_2S_4$ deposition was completed. The deposited mass of $NiCo_2S_4$ sample with SILAR cycles of 5, 9, and 14, was found to be 0.18, 0.20, and 0.23 mg cm^{-2}, respectively. The products attained using 5, 9, and 14, SILAR cycles were identified as NCS-05, NCS-09, and NCS-14, respectively [37].

2.3 Characterization

The crystal structure of the prepared samples was characterized by X-ray diffraction (XRD) using a Rigaku D/Max-KA X-ray diffractometer with Cu–K_α radiation. X-ray photoelectron spectroscopy (XPS; ULVAC-PHI Quantera SXM) and field emission scanning electron microscopy (FE-SEM; Hitachi, Model SU-70) were used to examine the surface morphology and nanostructures of synthesized $NiCo_2S_4$ samples. The nanostructures of the prepared $NiCo_2S_4$ samples were visualized by high-resolution transmission electron microscopy (TEM; JEOL, Model JEM-2100) [38]. For further characterization, the Raman and Fourier transform infrared (FT-IR) spectra of the prepared samples were also acquired.

2.4 Preparation and electrochemical testing of $NiCo_2S_4$ electrodes

The electrochemical properties of the supercapacitors were tested using an as-synthesized $NiCo_2S_4$ thin film as a working electrode, which was synthesized at different SILAR cycles, as described elsewhere [37]. A three-electrode system, which included a $NiCo_2S_4$ electrode as the working electrode, Pt as the counter electrode, and Ag/AgCl electrode as the reference electrode, was used to assess the electrochemical performance of the as-prepared $NiCo_2S_4$ electrodes. The working electrode probe was connected to the flexible stainless-steel substrate. The reference electrode probe was connected to an Ag/AgCl electrode, and the counter electrode probe was connected to a thin Pt electrode. The working electrode probe connected to the $NiCo_2S_4$/flexible stainless-steel electrode was immersed in 3 M KOH electrolyte solution. The supercapacitor properties were tested in the potential window -0.2 to 0.6 V. EIS tests were performed between 1 and 100 kHz, with AC amplitude of 10 mV and bias potential of 0.34 V. In electrochemical testing experiments, cyclic voltammetry (CV), galvanostatic charge/discharge, and EIS measurements were performed with a CHI 660E electrochemical workstation in aqueous 3 M KOH electrolyte [7].

3. Results and Discussion

3.1. FE-SEM and TEM analysis

FE-SEM and TEM are important tools used in determining the porosity and surface morphology of nanostructured materials [16]. Figure 1 (a–c) presents the FE-SEM micrographs of $NiCo_2S_4$ samples deposited at 5, 9, and 14 deposition cycles (the micrograph corresponding to 20 cycles is shown in Figure S1). In this paper, we synthesized flexible nanoflakes-like $NiCo_2S_4$ nanostructures of varying thickness and assessed the effect on electrochemical performance [32]. Figure 1a displays a typical FE-SEM micrograph of $NiCo_2S_4$ samples after five deposition cycles, evidencing the growth of the nanoflakes-like $NiCo_2S_4$ nanostructure formed on flexible stainless-steel substrate. The resulting nanostructure was uniform, and the flexible stainless-steel substrate was well-covered by the $NiCo_2S_4$ particles. Nonetheless, the sample lacked a specific surface morphology, due to the low number of deposition cycles (5 cycles). After increasing the number of cycles from 5 to 9, the $NiCo_2S_4$ sample exhibits a uniform distribution of interconnected nanosheets-like nanostructures on the stainless-steel substrate (as shown in Figure 1b) [39]. We observed that the interconnected nanosheets are vertically aligned on the stainless-steel substrate, and have an average thickness of about 30–50 nm and length of 300–400 nm [40]. This type of nanostructure is more beneficial than the NCS-05 sample for the ion transformation process during the electrochemical testing. Further increasing the number of deposition cycles from 9 to 14, a thicker $NiCo_2S_4$ sample was obtained compared to the previous two samples (NCS-05 and NCS-09), owing to the higher deposition cycle (as shown in Figure 1c). Following this deposition cycle, we confirmed collapse of the $NiCo_2S_4$ electrode, as shown in Figure S1. This result shows that the deposition cycle plays a significant role in optimizing the

$NiCo_2S_4$ electrode for supercapacitors, due to the loading capacitance of the active material and flexible stainless-steel substrate.

After confirmation of the FE-SEM result, we used TEM analysis to gain a detailed insight into the surface morphology of the $NiCo_2S_4$ samples. Figure 1 (d-f) provides the TEM images of the $NiCo_2S_4$ samples obtained after 9, 14, and 19 deposition cycles. The TEM image of the nanoplates-like $NiCo_2S_4$ sample synthesized by five deposition cycles had an average nanoplate thickness and length of 80-100 and 300–400 nm, respectively (Figure 1d). Furthermore, Figure 1e highlights the porous surface of the interconnected $NiCo_2S_4$ nanosheets, suggesting the nanosheets provided a high surface area between the $NiCo_2S_4$ electrode/electrolyte interfaces. This type of surface morphology benefits the ion/charge transportation in a supercapacitor with $NiCo_2S_4$ electrodes [41, 42]. At deposition cycle 14, the TEM shows that the nanoflakes-like morphology covers the nanoplates, all TEM micrographs are parallel the FE-SEM results. Figure 1 (g-i) shows the elemental mappings of the optimized $NiCo_2S_4$ sample, which is deposited at 9 SILAR cycle. All elemental mapping micrographs illustrate the uniform distribution of Ni, Co, and S elements on the flexible stainless-steel substrate, thereby implying uniformity of the $NiCo_2S_4$ thin films on the substrate [40-42].

The energy dispersive X-ray spectrometry technique was used to confirm the elemental and chemical composition of the $NiCo_2S_4$ samples. Figure 2 (a-c) is the EDS image of the $NiCo_2S_4$ sample synthesized at 5, 9, and 14 deposition cycles, and Figure S1 displays the EDS of the $NiCo_2S_4$ sample synthesized by 20 deposition cycles. From the EDS results, we verified the existence of Ni, Co, and S elements in all samples. Collectively, the FE-SEM, TEM, and EDS data proved the formation of phase-pure $NiCo_2S_4$ nanosheets-like material [42, 43].

3.2 XRD analysis

XRD allows identification of the phases and crystallinity of materials. The XRD pattern of the $NiCo_2S_4$ sample synthesized using nine SILAR cycles (Figure 3a) confirms the films have a cubic phase. The characteristic diffraction peaks at 26.04°, 30.99°, 37.62°, 62.33°, and 65.09°, correspond to the (220), (311), (400), (620), and (533) planes of cubic crystal phase $NiCo_2S_4$ nanomaterial (JCPDS 20-0782). Two weak peaks at 35.06°, 35.98° and 39.83° can be assigned to the (121), (301) and (102) of Co_9S_8 (JCPDS 11-0125). The relatively weak peak intensity of Co_9S_8 suggests this phase has poor crystallinity or is weaker than the $NiCo_2S_4$ phase [42]. Additionally, the four characteristic peaks at 43.94°, 44.92°, 50.92° and 75.01° originate from the stainless-steel substrate [38]. These results reveal the dominance of the strong $NiCo_2S_4$ material and no other material matching NiS, NiO, and NiCoO are present. After confirming that the as-obtained sample is principally $NiCo_2S_4$, we used Raman analysis to gain additional information about the composition and structure of the prepared $NiCo_2S_4$ samples.

Figure 3b displays a typical Raman spectrum of the $NiCo_2S_4$ nanosheets samples deposited on flexible stainless-steel substrate. The four main characteristic peaks at 458.32, 542.45, 614.34, and 623.54 cm^{-1} correspond to the F_2 stretching modes. Similar spectra and peak positions are observed in previous works [38, 44, 45]. The FT-IR spectrum of the $NiCo_2S_4$ thin film (Figure 3c) illustrates an intense band at 3415 cm^{-1}, representing the stretching vibration modes of the hydroxyl group (–OH). The peak at 1629 cm^{-1} is assigned to the COOH groups of C=O stretching vibrational modes [46], and the 1145 and 1096 cm^{-1} bands are due to the C–OH and C–O vibrational modes, respectively. The absorption bands at 633 and 588 cm^{-1} can be attributed to Ni–OH/S and Co–OH/S vibrational modes, respectively [47, 48].

3.3. XPS analysis

The chemical bonding states and elemental composition of the as-synthesized samples were established by XPS analysis. Figure 4 is a survey scan spectrum of the $NiCo_2S_4$ thin film, which indicates a predominance of C, S, O, Ni, and Co [49]. The O1s peak is essentially ascribed to surface adsorbed oxygen derived from preparing the sample in water and the air atmospheric condition [49]. The typical spectra of Ni 2p (Figure 4b) and Co 2p (Figure 4c) confirm the two spin-orbit doublets, respectively. In Figure 4b, which is related to the Ni 2p spectrum, the peaks positioned at 856.66 and 875.83 eV are from the Ni $2p_{3/2}$ and Ni $2p_{1/2}$, respectively. Correspondingly, the Co 2p spectrum in Figure 4c displays peaks at about 783.41 and 802.54 eV that are related to Co 2p, and the peak at 798.59 eV corresponds to the Co 3p [43, 49, 50]. Figure 4d depicts the typical spectra of S 2p, indicating the presence of sulfide ions in the ternary Ni-Co-S. The main peak of S 2p is located at 169.10 eV. These observed results are comparable to the earlier findings [41, 43-59]. In addition, C ls and O 1s are noted in the as-synthesized $NiCo_2S_4$ sample, due to the oxygen absorption on the surface of the sample (shown in Figure 4 (e, f)). The XPS results identify the atomic ratio of Ni, Co, and S elements in the $NiCo_2S_4$ nanoflakes is 1:1.94:3.95, which agrees with the reported output of $NiCo_2S_4$ electrodes. The XPS and XRD data are congruent, regarding the chemical composition, elemental state, and formation of pure $NiCo_2S_4$ phase. Moreover, the XPS indicates a mixed chemical composition involving Ni 2p/Ni 3p and Co 2p/Co 3p, which play an main role in enhancing the overall electrochemical performance of the $NiCo_2S_4$ electrode.

3.4. Electrochemical testing

For examination of the effect of deposition cycle number on the electrochemical attributes of $NiCo_2S_4$ electrodes, we used CV, galvanostatic charge/discharge, and EIS. The supercapacitor electrochemical testing of interconnected nanoplates-, nanosheets-, and

nanowire/nanoflakes-like $NiCo_2S_4$ electrodes were studied in 3 M KOH electrolyte, by using a three-electrode system [1]. Figure 5 (a–c) provides the CV curves of $NiCo_2S_4$ electrodes deposited using 5, 9, and 14 SILAR cycles on flexible stainless-steel substrate, coded as NCS-05, NCS-09, and NCS-14, respectively [10-16]. The supercapacitor properties were tested in the range -0.2–0.6 V, at a scan rate of 5–200 mV s^{-1}. Figure 5 shows the SILAR cycles influenced the supercapacitive properties of $NiCo_2S_4$ electrodes. NCS-9 had superior capability compared to NCS-5 and NCS-14, attributed to the higher areal surface of the three-dimensional (3D) interconnected nanosheets of the $NiCo_2S_4$ electrode and the ease at which ions are transferred from the very thin nanosheets. Figure 5d shows the specific capacitance of $NiCo_2S_4$ thin films deposited at different SILAR cycles, as a function of the scan rate of 5–200 mV s^{-1}. The interconnected nanoplates, nanosheets, and nanoflakes possess a specific capacitance of 766, 1076, and 921 F g^{-1} at 5 mV s^{-1}, respectively. Among the samples, the nanosheets-like nanostructure shows the best performance because of its very thin and long sheets. This type of nanostructure benefits the Co^{2+}/Co^{3+} and Ni^{2+}/Ni^{+3} ion exchange process during the electrochemical testing of $NiCo_2S_4$ samples, which concurred with the XPS results [1-5, 51]. The galvanostatic discharge curves of the $NiCo_2S_4$ thin films prepared at different deposition cycle with various current density from 1–8 mA cm^{-2}. Figure 6 (a–c) indicate NCS-09 has an extended charging/discharging capacity. The calculated specific capacitances are 634, 1326, and 736 F g^{-1} for NCS-5, NCS-9, and NCS-14 at 1 mA cm^{-2}, respectively (shown in Figure 6d). After comparison of the calculated specific capacitances, we confirmed the higher capacitance of NCS-09, which was two-fold more than the NCS-05 and NCS-14 samples, respectively. The outstanding specific capacitance value of the NCS-09 sample is reported elsewhere [1, 16-19]. Table 1 compares the $NiCo_2S_4$ electrodes synthesized by the different SILAR cycles. The

association between the solution resistance, charge transfer resistance, and Warburg constants was examined using the EIS technique. Figure 7 represents the Nyquist plots of $NiCo_2S_4$ electrodes prepared using different SILAR cycles, and the inset shows the fitted results. The fitted results (Figure 7, inset) corroborate the electrochemical data of the equivalent circuit. The solution resistances of NCS-05, NCS-09, and NCS-14 samples were 6.05, 5.40, and 6.51 Ω, and the charge transferred resistances were 10.28, 6.76, and 5.18 Ω, respectively. The NCS-09 possesses the lower average resistance among the samples, which specifies that the nanosheets-like $NiCo_2S_4$ sample [5], which is deposited at the 14 SILAR cycles [51, 52], is more conductive.

4. Conclusions

In summary, hierarchical 3D interconnected nanosheets-like $NiCo_2S_4$ electrodes were effectively synthesized using a facile chemical SILAR method for extending the supercapacitor applications. The supercapacitor testing reveals that the as-synthesized $NiCo_2S_4$ electrodes possess higher specific capacitance. The nanosheets-like $NiCo_2S_4$ electrodes exhibit a maximum capacitance of up to 1072 F g^{-1} at the scan rate of 5 mV cm^{-2}. The outstanding performance of the $NiCo_2S_4$ electrode is due to the 3D interconnected nanosheets-like $NiCo_2S_4$ nanostructure. The supercapacitor results of the 3D interconnected nanostructure of $NiCo_2S_4$ electrodes show it has great potential in the energy storage device.

Acknowledgment:

This work was supported by the Dongguk University Research Fund of 2018

References

[1] S. Chen, Y. Yang, Z. Zhan, J. Xie, J. Xiong, Designed construction of hierarchical $NiCo_2S_4$@polypyrrole core–shell nanosheet arrays as electrode materials for high-performance hybrid supercapacitors, RSC Adv., 7 (2017) 18447–18455.

[2] P. Simon, Y. Gogotsi, Materials for electrochemical capacitors, Nat. Mater., 7 (2008) 845–854.

[3] Y. Jiang, L. Zhang, H. Zhang, C. Zhang, S. Liu, Hierarchical $Ni_{0.54}Co_{0.46}O_2$ nanowire and nanosheet arrays grown on carbon fiber cloth for high-performance supercapacitors, J. Power Sources, 329 (2016) 473–483.

[4] W. Li, L. Xin, X. Xu, Q. Liu, M. Zhang, S. Ding, M. Zhao, X. Lou, Facile synthesis of three-dimensional structured carbon fiber-$NiCo_2O_4$-$Ni(OH)_2$ high-performance electrode for pseudocapacitors, Sci. Rep., 5 (2015) 9277.

[5] H. Wang, C. Wang, C. Qing, D. Sun, B. Wang, G. Qu, M. Sun, Y. Tang, Construction of carbon-nickel cobalt sulphide hetero-structured arrays, on nickel foam for high performance asymmetric supercapacitors, Electrochim Acta, 174 (2015) 1104–1112.

[6] W. Hu, R. Chen, W. Xie, L. Zou, N. Qin, D. Bao, $CoNi_2S_4$ nanosheet arrays supported on nickel foams with ultrahigh capacitance for aqueous asymmetric supercapacitor applications, ACS Appl. Mater. Interfaces, 6 (2014) 19318–19326.

[7] D.-Y. Kim, G. S. Ghodake, N. C. Maile, A. A. Kadam, Dae Sung Lee, V. J. Fulari, S. K. Shinde, Chemical synthesis of hierarchical $NiCo_2S_4$ nanosheets like nanostructure on flexible foil for a high performance supercapacitor, Sci. Rep., 7 (2017) 9764.

[8] J. Liu, J. Jiang, C. Cheng, H. Li, J. Zhang, H. Gong, H. J. Fan, Co_3O_4 nanowire@MnO_2 ultrathin nanosheet core/shell arrays: a new class of high-performance pseudocapacitive materials, Adv. Mater., 23 (2011) 2076–2081.

[9] W. Kong, C. Lu, W. Zhang, J. Pu, Z. Wang, Homogeneous core–shell $NiCo_2S_4$ nanostructures supported on nickel foam for supercapacitors, J. Mater. Chem. A, 3 (2015) 12452–12460.

[10] M. Wang, Y. Zhao, X. Zhang, R. Qi, S. Shi, Z. Li, Q. Wang, Y. Zhao, Interface-rich core–shell ammonium nickel cobalt phosphate for high-performance aqueous hybrid energy storage device without a depressed power density, Electrochim Acta, 272 (2018) 184–191.

[11] M. Wang, F. Jin, X. Zhang, J. Wang, S. Huang, X. Zhang, S. Mu, Y. Zhao, Y. Zhao, Multihierarchical structure of hybridized phosphates anchored on reduced graphene oxide for high power hybrid energy storage devices, ACS Sustainable Chem. Eng. 5 (2017) 5679−5685.

[12] Z. Chen, D.-B. Xiong, X. Zhang, H. Ma, M. Xia, Y. Zhao, Construction of a novel hierarchical structured NH_4-Co-Ni phosphate toward an ultrastable aqueous hybrid capacitor, Nanoscale, 8 (2016) 6636–6645.

[13] Y. Zhao, H. Ma, S. Huang, X. Zhang, M. Xia, Y. Tang, Z.-F. Ma, Monolayer nickel cobalt hydroxyl carbonate for high performance all-solid-state asymmetric supercapacitors, ACS Appl. Mater. Interfaces, 8 (2016) 22997−23005.

[14] B. Li, P. Gu, Y. Feng, G. Zhang, K. Huang, H. Xue, H. Pang, Ultrathin nickel–cobalt phosphate 2D nanosheets for electrochemical energy storage under aqueous/solid-state electrolyte, Adv. Funct. Mater. 27 (2017) 1605784.

[15] L. Shen, L. Du, S. Tan, Z. Zang, C. Zhao, W. Mai, Flexible electrochromic supercapacitor hybrid electrodes based on tungsten oxide films and silver nanowires, Chem. Commun., 52 (2016) 6296–6299.

[16] S. Zheng, X. Li, B. Yan, Q. Hu, Y. Xu, X. Xiao, H. Xue, H. Pang, Transition-metal (Fe, Co, Ni) based metal-organic frameworks for electrochemical energy storage, Adv. Energy Mater., 7 (2017) 1602733-1602760.

[17] Y. Xu, S. Zheng, H. Tang, X. Guo, H. Xue, H. Pang, Prussian blue and its derivatives as electrode materials for electrochemical energy storage, Energy Storage Materials, 9 (2017) 11–30.

[18] X. Xiao, S. Zheng, X. Li, G. Zhang, X. Guo, H. Xue, H. Pang, Facile synthesis of ultrathin Ni-MOF nanobelts for high-efficiency determination of glucose in human serum, J. Mater. Chem. B, 5 (2017) 5234–5239.

[19] Y. Xu, B. Li, S. Zheng, P. Wu, J. Zhan, H. Xue, Q. Xu, H. Pang, Ultrathin two-dimensional cobalt–organic framework nanosheets for high-performance electrocatalytic oxygen evolution, J. Mater. Chem. A., 2018, DOI: 10.1039/C8TA03128B.

[20] H. Qin, S. Yang, W. Zhao, Z. Yang, X. Li, H. Li, P. Yao, Synthesis of mesoporous $NiCo_2S_4$ deposited on reduced graphite oxide assistant by co-polymer Pluronic F127 for high-performance supercapacitor, Appl. Surf. Sci., 420 (2017) 77–82.

[21] H. Gu, W. Fan, T. Liu, Phosphorus-doped $NiCo_2S_4$ nanocrystals grown on electrospun carbon nanofibers as ultra-efficient electrocatalysts for the hydrogen evolution reaction, Nanoscale Horiz., 2 (2017) 277–283.

[22] K. Liang, W. He, X. Deng, H. Ma, X. Xu, Controlled synthesis of $NiCo_2S_4$ hollow spheres as high-performance electrode materials for supercapacitors, J. Alloy Compd, 735 (2018) 1395–1401.

[23] X. Chen, D. Chen, X. Guo, R. Wang, H. Zhang, Facile growth of caterpillar-like $NiCo_2S_4$ nanocrystal arrays on nickle [sic] foam for high-performance supercapacitors, ACS Appl. Mater. Interfaces, 9 (22) (2017) 18774–18781.

[24] W. Fu, C. Zhao, W. Han, Y. Liu, H. Zhao, Y. Ma, E. Xie, Cobalt sulfide nanosheets coated on $NiCo_2S_4$ nanotube arrays as electrode materials for high-performance supercapacitors, J. Mater. Chem. A, 3 (2015) 10492–10497.

[25] Y. Tao, L. Ruiyi, Z. Lin, M. Chenyang, L. Zaijun, Three-dimensional electrode of Ni/Co layered double hydroxides@$NiCo_2S_4$@graphene@Ni foam for supercapacitors with outstanding electrochemical performance, Electrochim. Acta, 176 (2015) 1153–1164.

[26] D. Wang, W. Zhu, Y. Yuan, G. Du, J. Zhu, X. Zhu, G. Pezzotti, Kelp-like structured $NiCo_2S_4$-C-MoS_2 composite electrodes for high performance supercapacitor, J. Alloy Compd., 735 (2018) 1505–1513.

[27] Y. Song, H. Li, L. Yang, D. Bai, F. Zhang, S. Xu, Solid-solution sulfides derived from tunable layered double hydroxide precursors/graphene aerogel for pseudocapacitors and sodium-ion batteries, ACS Appl. Mater. Interfaces, 9 (2017) 42742–42750.

[28] X. Cai, X. Shen, L. Ma, Z. Ji, L. Kong, Facile synthesis of nickel–cobalt sulfide/reduced graphene oxide hybrid with enhanced capacitive performance, RSC Adv., 5 (2015) 58777–58783.

[29] Q. Liu, J. Jin, J. Zhang, $NiCo_2S_4$@graphene as a bifunctional electrocatalyst for oxygen reduction and evolution reactions, ACS Appl. Mater. Interfaces, 5 (2013) 5002–5008.

[30] J. Zhang, H. Guan, Y. Liu, Y. Zhao, B. Zhang, Hierarchical polypyrrole nanotubes@$NiCo_2S_4$ nanosheets core–shell composites with improved electrochemical performance as supercapacitors, Electrochim. Acta, 258 (2017) 182–191.

[31] H. Wan, J. Liu, Y. Ruan, L. Lv, L. Peng, X. Ji, L. Miao, J. Jiang, Hierarchical configuration of $NiCo_2S_4$ nanotube@Ni−Mn layered double hydroxide arrays/three-dimensional graphene sponge as electrode materials for high-capacitance supercapacitors, ACS Appl. Mater. Interfaces, 7 (2015) 15840–15847.

[32] R. Li, S. Wang, Z. Huang, F. Lu, T. He, $NiCo_2S_4$@$Co(OH)_2$ core–shell nanotube arrays in situ grown on Ni foam for high performances asymmetric supercapacitors, J. Power Sources, 312 (2016) 156–164.

[33] T. He, S. Wang, F. Lu, M. Zhang, X. Zhang, L. Xu, Controllable synthesis of hierarchical $NiCo_2S_4$@Ni_3S_2 core–shell nanotube arrays with excellent electrochemical performance for aqueous asymmetric supercapacitors, RSC Adv., 6 (2016) 97352–97362.

[34] L. Niu, Y. Wang, F. Ruan, C. Shen, S. Shan, M. Xu, Z. Sun, C. Li, X. Liu, Y. Gong, *In situ* growth of $NiCo_2S_4$@$Ni_3V_2O_8$ on Ni foam as a binder-free electrode for asymmetric supercapacitors, J. Mater. Chem. A, 4 (2016) 5669–5677.

[35] X. Wu, S. Li, B. Wang, J. Liu, M. Yu, *In situ* template synthesis of hollow nanospheres assembled from $NiCo_2S_4$@C ultrathin nanosheets with high electrochemical activities for lithium storage and ORR catalysis, Phys. Chem. Chem. Phys., 19 (2017) 11554–11562.

[36] M. Yao, Z. Hu, Y. Liu, P. Liu, Design and synthesis of hierarchical $NiCo_2S_4$@$NiMoO_4$ core/shell nanospheres for high-performance supercapacitors, New J. Chem., 39 (2015) 8430–8438.

[37] S. K. Shinde, D. P. Dubal, G. S. Ghodake, D. Y. Kim, V. J. Fulari, Nanoflower-like CuO/$Cu(OH)_2$ hybrid thin films: synthesis and electrochemical supercapacitive properties, J. Electroanal. Chem., 732 (2014) 80–85.

[38] Z. Zhang, Q. Li, Z. Li, J. Ma, C. Li, L. Yin, X. Gao, Partially reducing reaction tailored mesoporous 3D carbon coated NiCo-$NiCoO_2$/Carbon xerogel hybrids as anode materials for lithium ion battery with enhanced electrochemical performance, Electrochim. Acta, 203 (2016) 117–127.

[39] V. H. Nguyen, J.-J. Shim, Three-dimensional nickel foam/graphene/$NiCo_2O_4$ as high-performance electrodes for supercapacitors, J. Power Sources, 273 (2015) 110–117.

[40] J. Pu, T. Wang, H. Wang, Y. Tong, C. Lu, W. Kong, Z. Wang, Direct growth of $NiCo_2S_4$ nanotube arrays on nickel foam as high-performance binder-free electrodes for supercapacitors, Chem. Plus. Chem., 79 (2014) 577–583.

[41] W. Xiong, Z. Guo, H. Li, R. Zhao, X. Wang, Rational bottom-up engineering of electrocatalysts by atomic layer deposition: a case study of $Fe_xCo_{1-x}S_y$-based catalysts for electrochemical hydrogen evolution, ACS Energy Lett., 2 (2017) 2778–2785.

[42] H. Wang, Q. Ren, D. J. L. Brett, G. He, R. Wang, J. Key, S. Ji, Double-shelled tremella-like $NiO@Co_3O_4@MnO_2$ as a high-performance cathode material for alkaline supercapacitors, J. Power Sources, 343 (2017) 76–82.

[43] W. Hu, R. Chen, W. Xie, L. Zou, N. Qin, D. Bao, $CoNi_2S_4$ nanosheet arrays supported on nickel foams with ultrahigh capacitance for aqueous asymmetric supercapacitor applications, ACS Appl. Mater. Interfaces, 6 (2014) 19318–19326.

[44] D. Zhang, H. Yan, Y. Lu, K. Qiu, C. Wang, Y. Zhang, X. Liu, J. Luo, Y. Luo, $NiCo_2O_4$ nanostructure materials: morphology control and electrochemical energy storage, Dalton Trans., 43 (2014) 15887–15897.

[45] Z. Zeng, D. Wang, J. Zhu, F. Xiao, Y. Li, X. Zhu, $NiCo_2S_4$ nanoparticles//activated balsam pear pulp for asymmetric hybrid capacitors, CrystEngComm, 18 (2016) 2363–2374.

[46] X. Cai, X. Shen, L. Ma, Z. Ji, C. Xu, A. Yuan, Solvothermal synthesis of NiCo-layered double hydroxide nanosheets decorated on RGO sheets for high performance supercapacitor, Chem. Eng. J., 268 (2015) 251–259.

[47] H. Gao, G. Wang, M. Yang, L. Tan, J. Yu, Novel tunable hierarchical Ni–Co hydroxide and oxide assembled from two-wheeled units, Nanotechnology 23 (2012) 15607-15615.

[48] S. Deabate, F. Fourgeot, F. Henn, X-ray diffraction and micro-Raman spectroscopy analysis of new nickel hydroxide obtained by electrodialysis, J. Power Sources, 87 (2000) 125–136.

[49] J. Zhao, Z. Li, M. Zhang, A. Meng, Q. Li, Vertically cross-linked and porous $CoNi_2S_4$ nanosheets-decorated SiC nanowires with exceptional capacitive performance as a free-standing electrode for asymmetric supercapacitors, J. Power Sources, 332 (2016) 355–365.

[50] Z. Liu, L. Wang, Y. F. Cheng, X. Cheng, B. Lin, L. Yue, S. Chen, Facile synthesis of $NiCo_{2-x}Fe_xO_4$ nanotubes/carbon textiles composites for high-performance electrochemical energy storage devices, ACS Appl. Nano Mater., 2 (2018) 997–1002.

[51] D. Cai, D. Wang, C. Wang, B. Liu, L. Wang, Y. Liu, Q. Li, T. Wang, Construction of desirable $NiCo_2S_4$ nanotube arrays on nickel foam substrate for pseudocapacitors with enhanced performance, Electrochim. Acta, 151 (2015) 35–41.

[52] D. Li, Y. Gong, C. Pan, Facile synthesis of hybrid CNTs/$NiCo_2S_4$ composite for high performance supercapacitors, Sci. Rep., 6 (2016) 29788.

Figure capation

Figure 1 FE-SEM, TEM and electromapping images of $NiCo_2S_4$ nanostructures depositing by different SILAR cycles on flexible stainless-steel substrate.

Figure 2 EDS image of $NiCo_2S_4$ nanostructures depositing by different SILAR cycles on flexible stainless-steel substrate.

Figure 3 XRD, Raman and FT-IR of obtained $NiCo_2S_4$ thin film synthesized using 09 SILAR cycles on flexible stainless-steel substrate

Figure 4 XPS of $NiCo_2S_4$ electrode synthesized by 09 SILAR cycles on flexible stainless-steel substrate

Figure 5 CV and specific capacitance of the $NiCo_2S_4$ nanostructures depositing by different SILAR cycles on flexible conducting electrode.

Figure 6 GCD and specific capacitance of the $NiCo_2S_4$ nanostructures depositing by different SILAR cycles on flexible conducting electrode.

Figure 7 EIS of the $NiCo_2S_4$ nanostructures depositing by different SILAR cycles on flexible conducting electrode, inset show the fitted and experimental results.

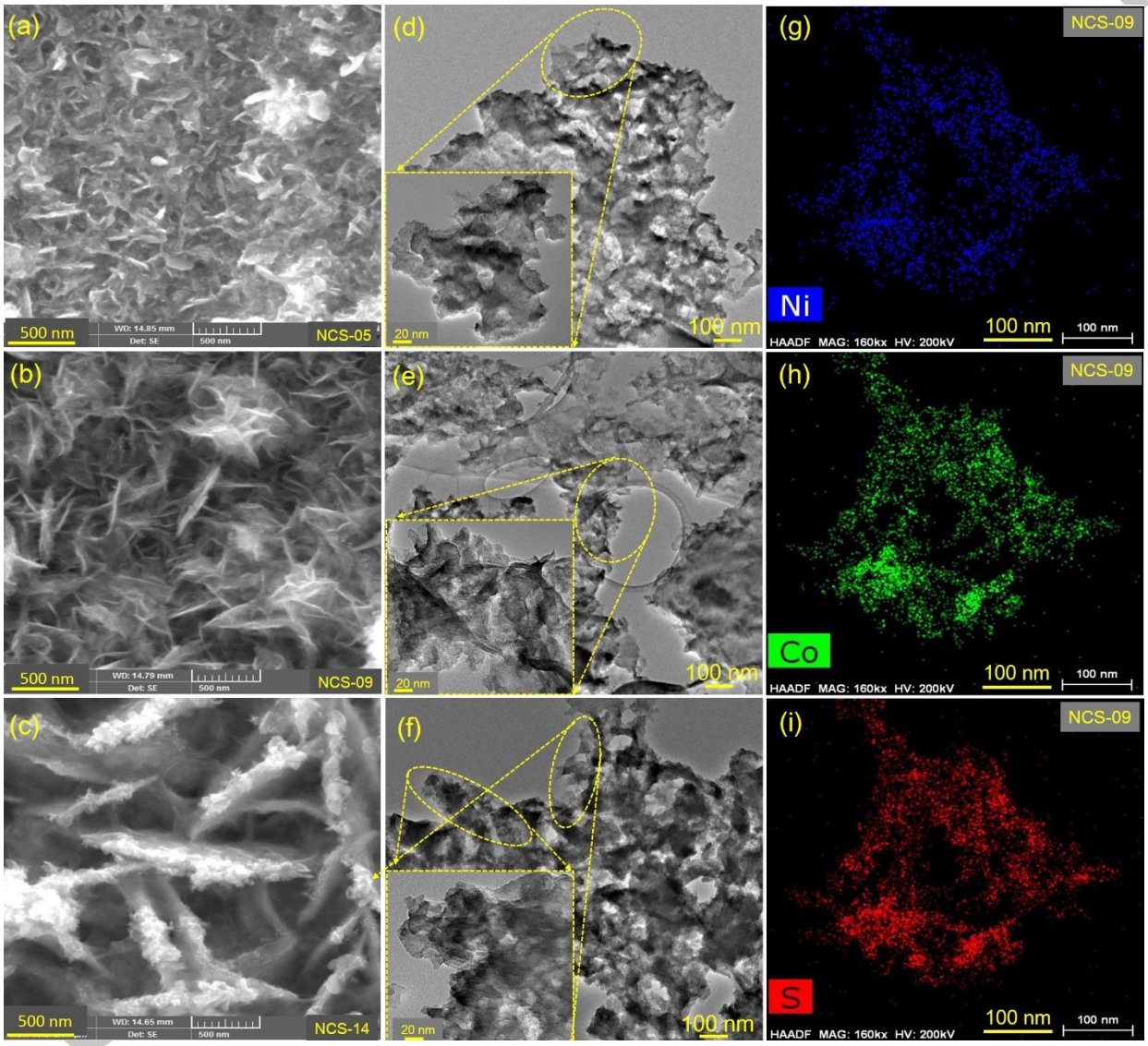
(a)
500 nm
NCS-05
(b)
500 nm
NCS-09
(c)
500 nm
NCS-14
(d)
20 nm
100 nm
(e)
20 nm
100 nm
(f)
20 nm
100 nm
(g)
NCS-09
Ni
100 nm
HAADF MAG: 160kx HV: 200kV
(h)
NCS-09
Co
100 nm
HAADF MAG: 160kx HV: 200kV
(i)
NCS-09
S
100 nm
HAADF MAG: 160kx HV: 200kV

Figure 1

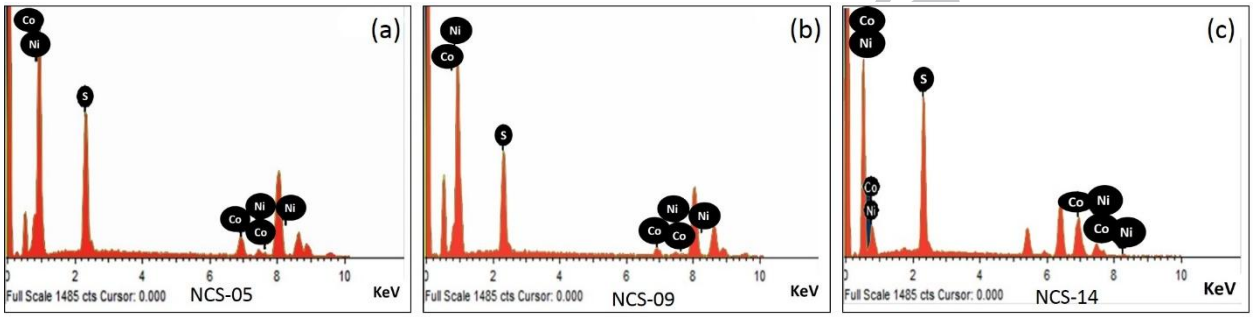

Figure 2

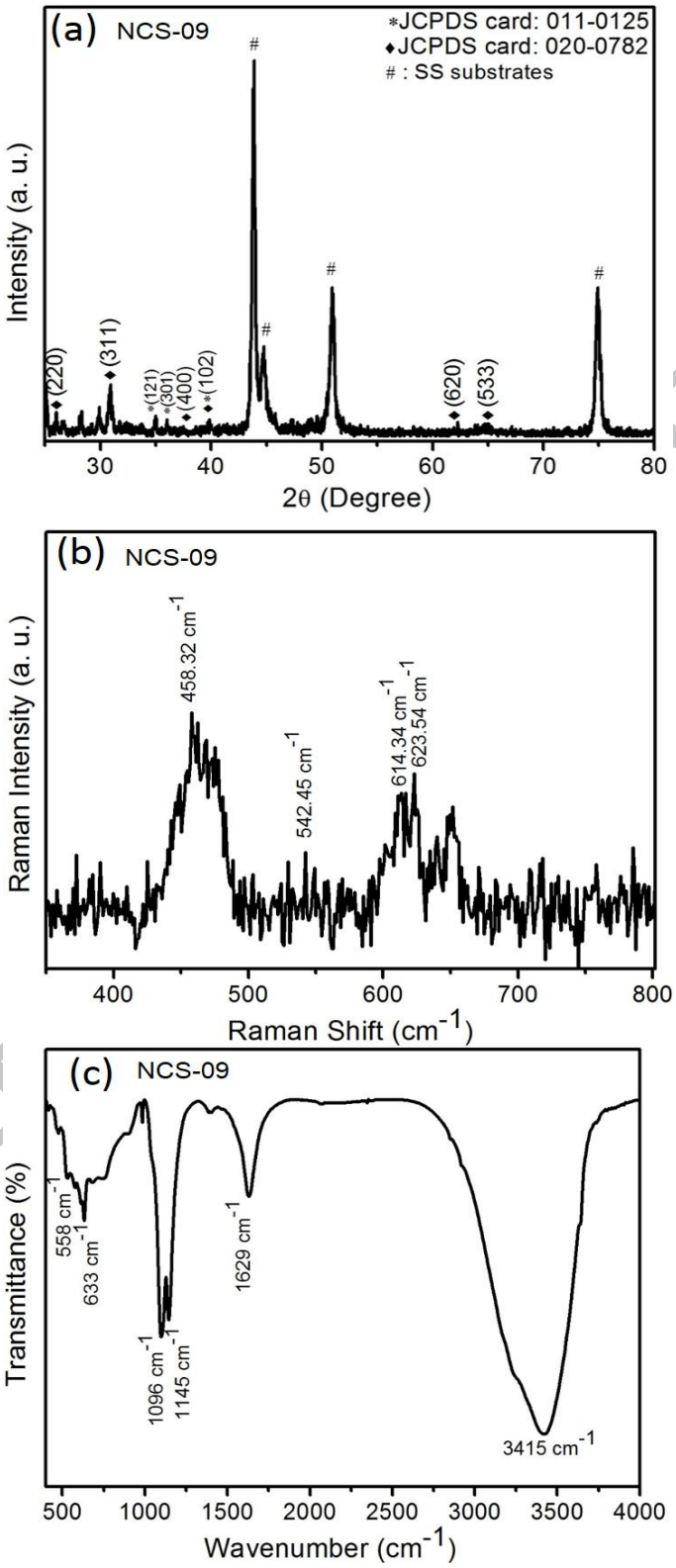
(a) NCS-09
*JCPDS card: 011-0125
♦JCPDS card: 020-0782
: SS substrates
Intensity (a. u.)
(220)
(311)
*(121)
*(301)
♦(400)
*♦(102)
#
(620)
(533)
30
40
50
60
70
80
2θ (Degree)
(b) NCS-09
Raman Intensity (a. u.)
458.32 cm-1
542.45 cm-1
614.34 cm-1
623.54 cm-1
400
500
600
700
800
Raman Shift (cm-1)
(c) NCS-09
Transmittance (%)
558 cm-1
633 cm-1
1096 cm-1
1145 cm-1
1629 cm-1
3415 cm-1
500
1000
1500
2000
2500
3000
3500
4000
Wavenumber (cm-1)

Figure 3

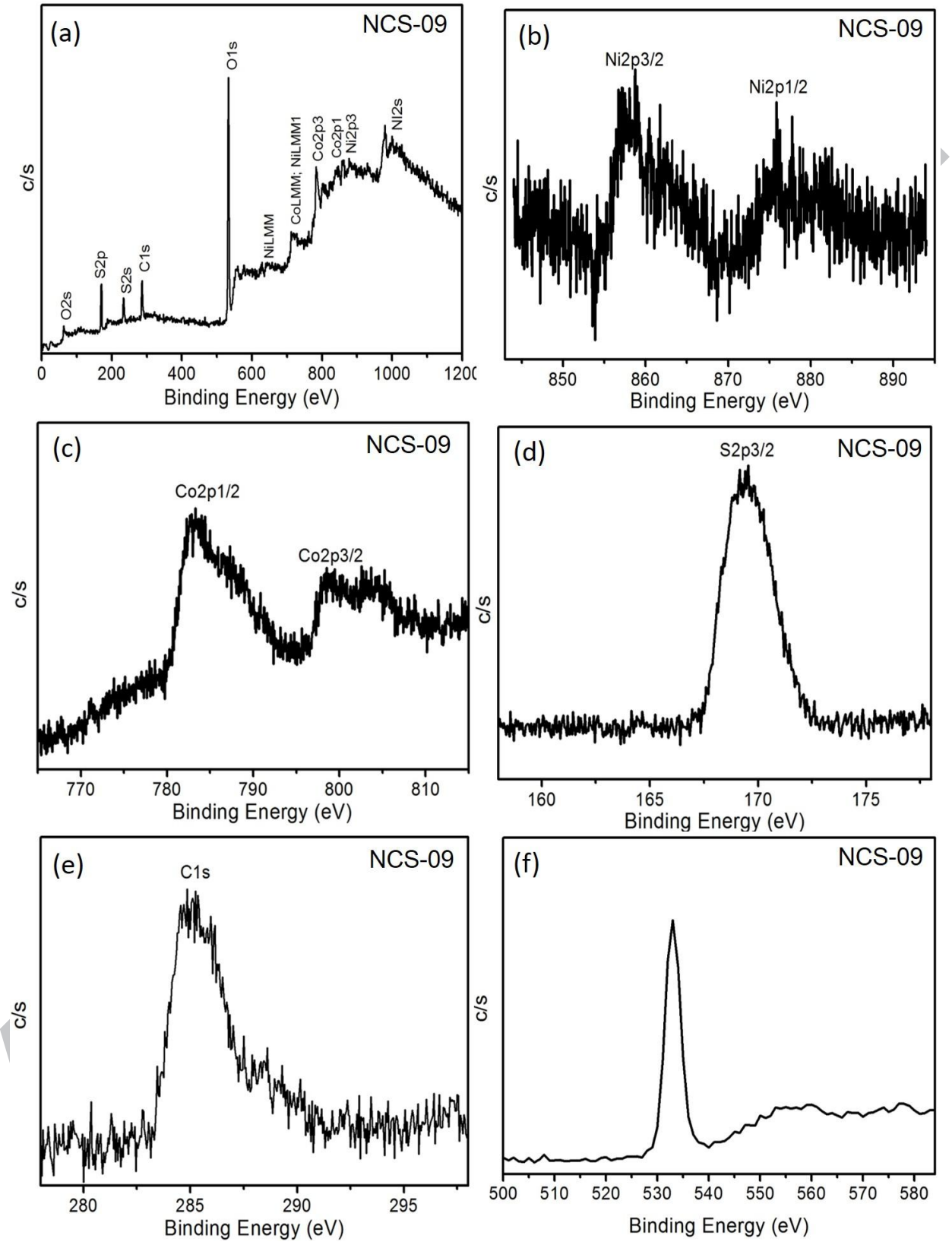
(a)
NCS-09
O1s
NiLMM
CoLMM; NiLMM1
Co2p3
Co2p1
Ni2p3
NI2s
S2p
S2s
C1s
O2s
c/s
Binding Energy (eV)
(b)
NCS-09
Ni2p3/2
Ni2p1/2
c/s
Binding Energy (eV)
(c)
NCS-09
Co2p1/2
Co2p3/2
c/s
Binding Energy (eV)
(d)
NCS-09
S2p3/2
c/s
Binding Energy (eV)
(e)
NCS-09
C1s
c/s
Binding Energy (eV)
(f)
NCS-09
c/s
Binding Energy (eV)

Figure 4

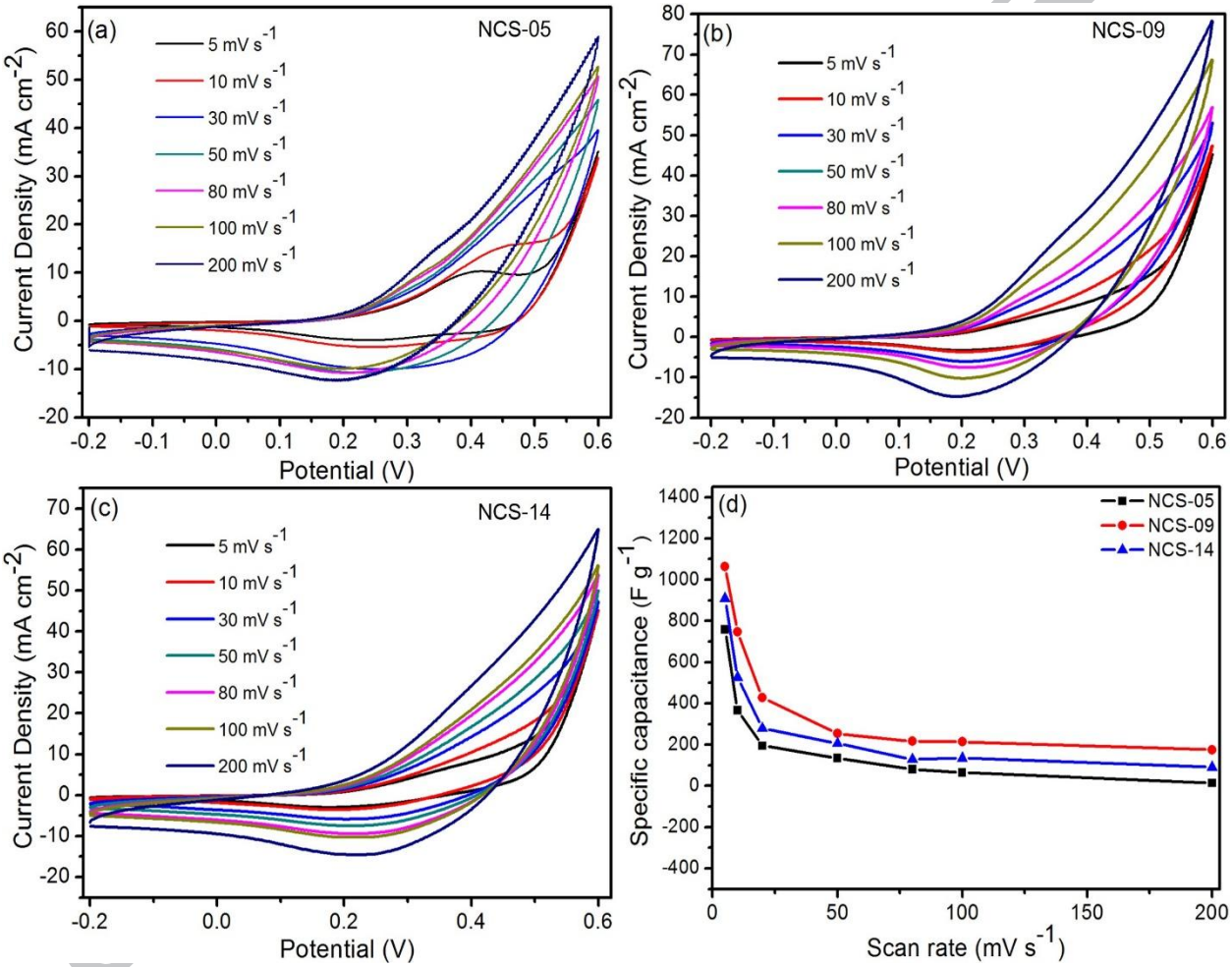

Figure 5

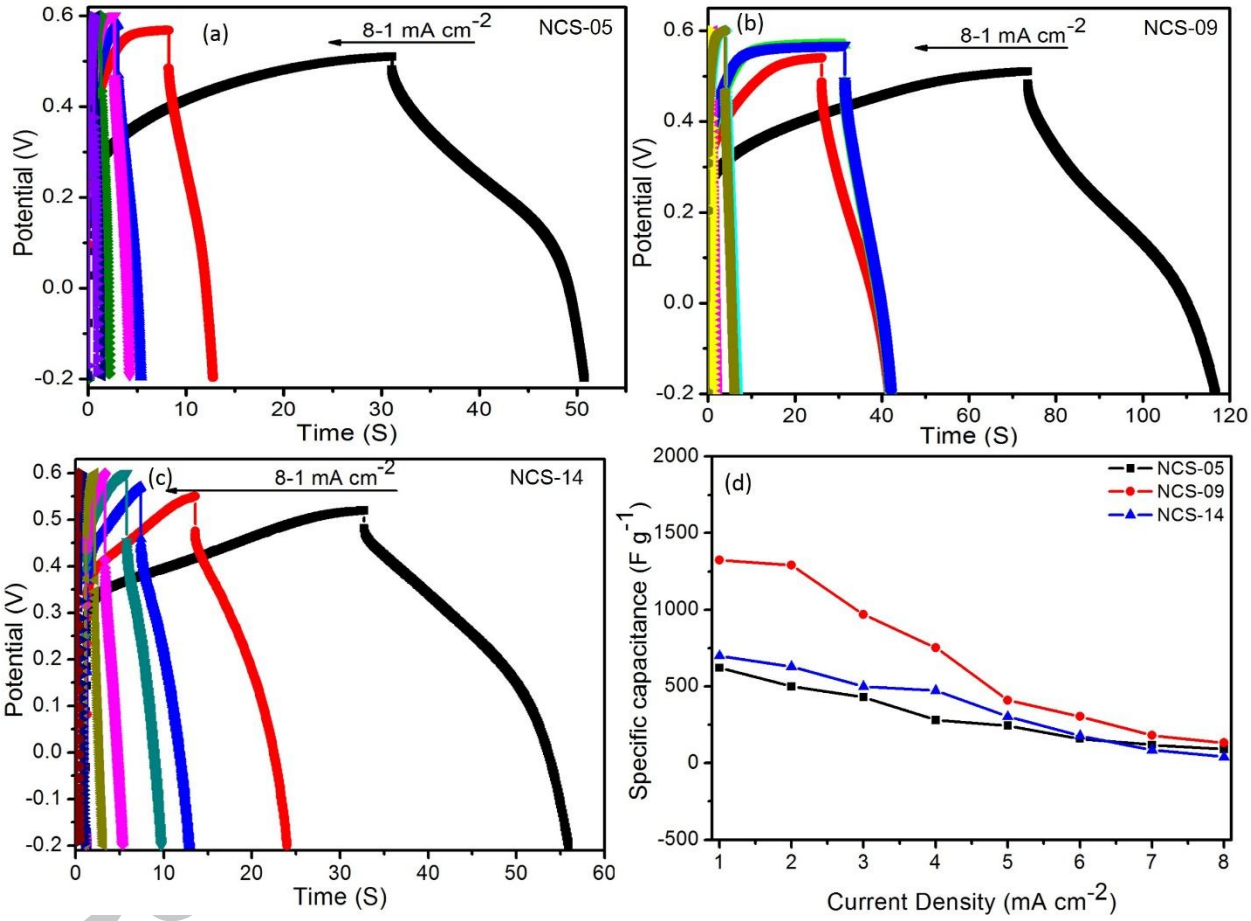

Figure 6

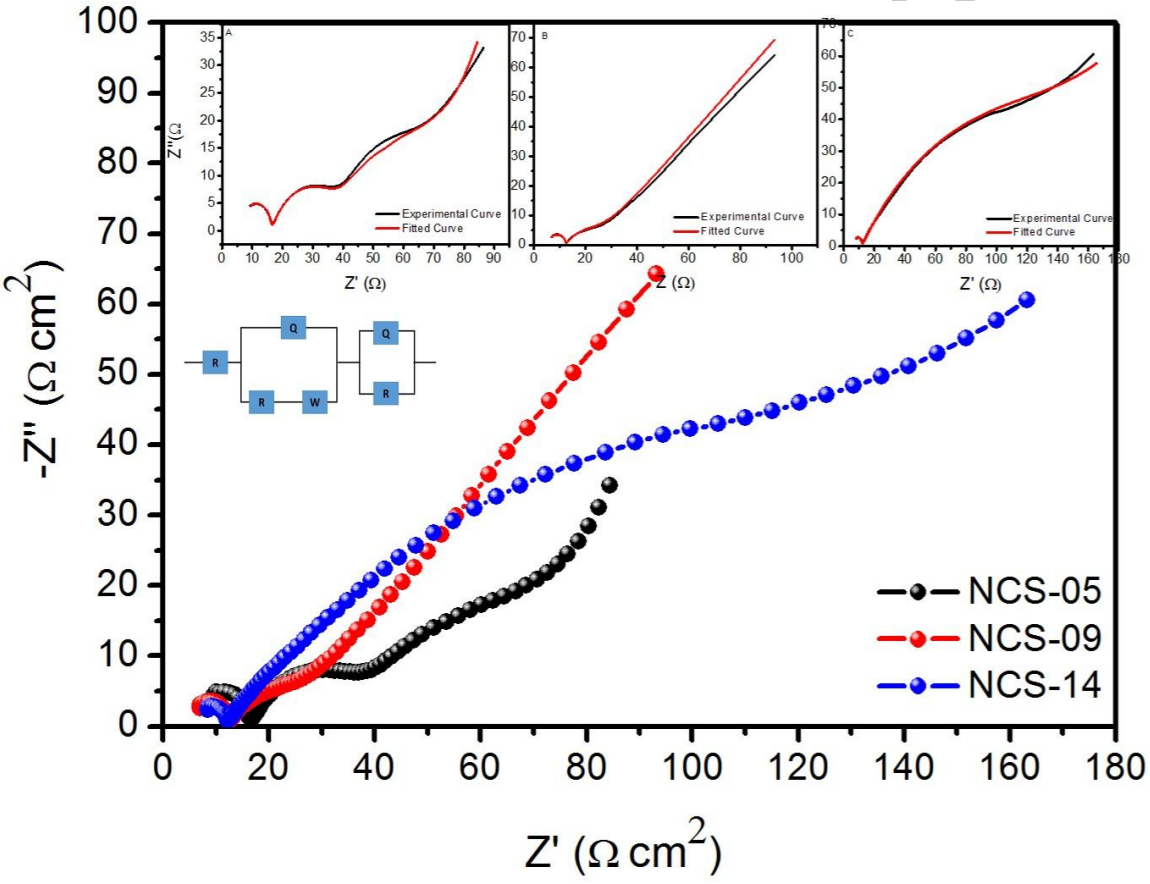

Figure 7

Table Caption

Table 1 Electrochemical parameter of $NiCo_2S_4$ electrode synthesized different nanostructure using SILAR cycle.

Name of samples	NCS-05	NCS-09	NCS-15
R_1	6.05	5.40	6.51
Q-Y_o	5.216e-8	6.273e-7	6.066e-8
Q-n	0.96	1.0	1.0
R_2	10.28	6.76	5.18
W	0.028	0.012	0.025
Q-Y_o	0.00046	0.00175	0.002711
Q-n	0.69	0.61	0.50
R_3	22.32	11.92	149.6

❖ Research Highlights

- Novel route for the synthesis of $NiCo_2S_4$ thin films
- Different nanostructure of $NiCo_2S_4$ thin films
- NCS-09 shows the more surface area
- NCS-09 shows excellent supercapacitive properties

Graphical Abstract:

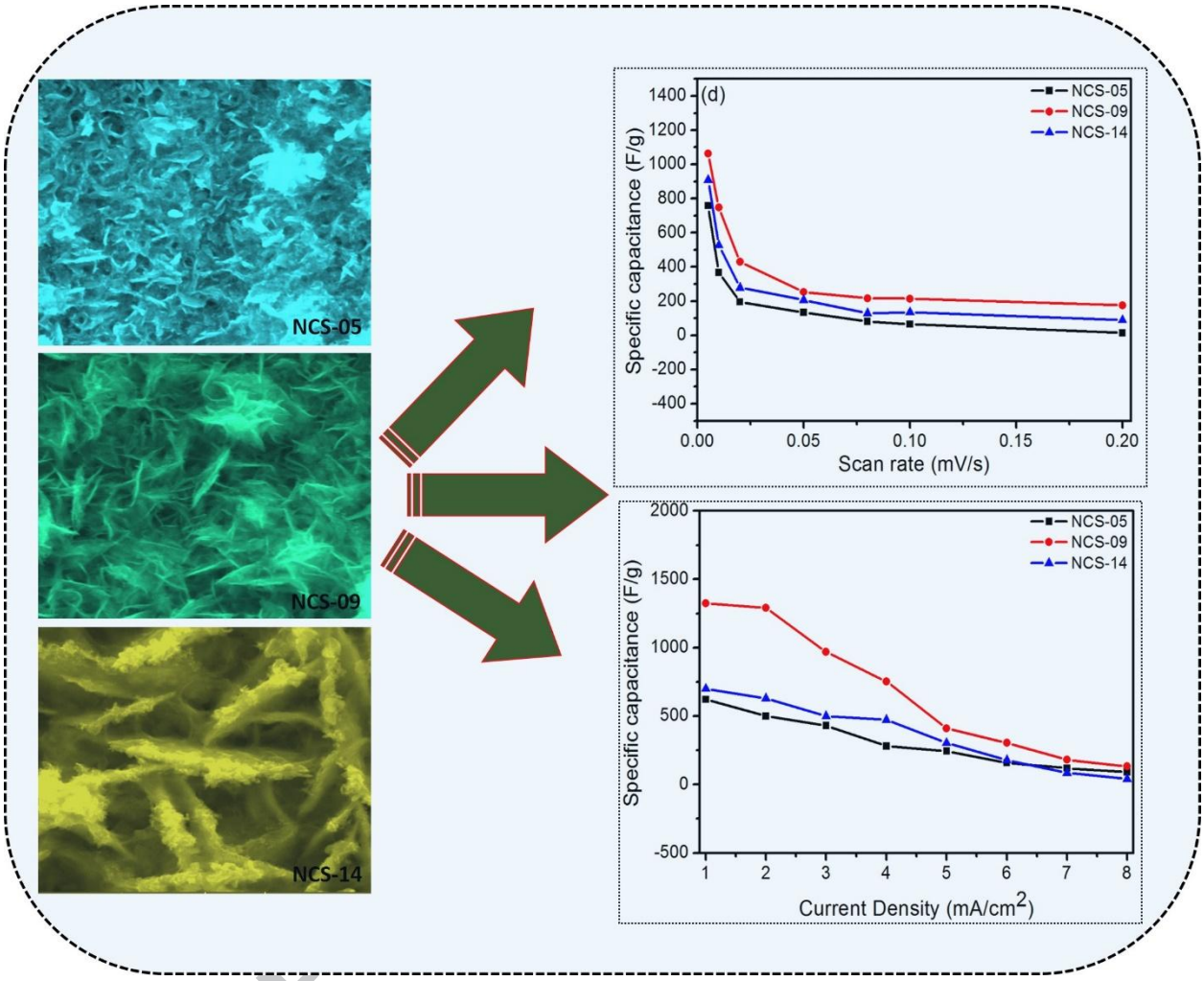

FE-SEM images and specific capacitance of $NiCo_2S_4$ electrodes deposited at various SILAR cycle and nominated at NCS-05, NCS-09, and NCS-14 respectively.